RSC Advances

ROYAL SOCIETY OF CHEMISTRY

www.rsc.org/advances

Submitted to RSC Advances

Exceptional electrical and thermal transport properties in tunable all-graphene papers

Lin Liu[†], Xing-Ming Bian[†,*], Jin Tang[†], Hong Xu[†], Zhi-Ling Hou[§,*], Wei-Li Song[‡,*]

[†]*State Key Laboratory of Alternate Electrical Power System with Renewable Energy Sources, North China Electric Power University, Beijing, 102206, China*

[‡]*Institute of Advanced Materials and Technology, University of Science and Technology Beijing, Beijing 100083, China*

[§]*School of Science, Beijing University of Chemical Technology, Beijing 100029, China*

* Corresponding Authors: bianxingming@ncepu.edu.cn (X. M. B.); houzl@mail.buct.edu.cn (Z. L. H.); weilis@ustb.edu.cn (W. L. S.).

Abstract

Lightweight thermally conductive materials of various electrical features, ranging from insulators such as boron nitride composites to highly conductive graphene-based mateirals, are increasingly attractive in substituting traditional metal materials for many practical applications. Herein we take a new insight into the electrical and thermal transport properties of the flexible all-graphene papers, where electrically and thermally insulating graphene oxide nanosheets (GO) serve as unique interfaces in the graphene papers stacked by electrically and thermally conductive graphene nanosheets (GN). The anisotropic all-graphene papers with decoupling of thermal and electrical transport properties have been achieved based on controlling the electron and phonon transport paths at the GN-GO interfaces. The fundamental mechanism of the exclusive electrical and thermal transport behaviors in the all-graphene papers has been discussed, indicating more advantageous features in manipulating the transport properties in comparison with other conventional graphene/polymer composites. Implication of the tunable thermal conductivity in the entire semi-conductive range suggests a conceptually novel stage toward fabricating advanced graphene materials of various electrical features for wide thermal management.

Key words: graphene; electrical transport; thermal transport; interfacial management; semiconductors.

1. Introduction

Light-weight materials of thermal transport properties are urgently important to a variety of applications from high-performance electronics to the rapidly increasing demand in the effective thermal management systems, since heat removal has become a crucial issue for continuing progress in such industry.[1-4] The commonly used thermal transport metals like aluminum, copper and silver are rather heavy and generally suffer from the oxidation and corrosion, limiting the their long-term service in the corrosive environment. As the substitutes, light-weight thermally conductive composites based on carbon materials of effective phonon transport paths have been well developed since they occupy a unique place in terms of their ability to steady heat dissipation under certain extreme conditions.[1-4]

Among the carbon materials, two-dimensional graphene nanosheets of delocalized π electronic networks for excellent thermal and electrical conductivities have shown great potential in novel thermal management applications, specifically based on in-plane thermal conductivity up to thousands of W/mK units at the individual graphene level.[1,5-7] For achieving the goals in the bulk graphene/graphite materials, alignment of the graphene nanosheets is known to be an optimal approach to obtain extreme thermal transport along the in-plane direction.[8-11] For examples, Drazl and coworkers have used the exfoliated graphite nanoplates to fabricate free-standing papers with filtration technique, and the papers upon mechanical pressing and thermal annealing showed thermal conductivity up to 178 W/mK.[10] Later in the work by Kang and coworkers, graphitic blocks of natural graphite and mesophase pitch were fabricated using hot pressing for aligning the graphitic plates. The as-fabricated blocks with denser stacking and highly anisotropic feature exhibited an in-plane thermal conductivity of 522 W/mK.[11] Further modifications including utilization of graphene nanosheets with enhanced thermal conductivity[12,13] and high-temperature graphitization[13,14]

have essentially promoted the electrical and thermal conductivities of the resulting graphene papers.

Besides the advances in metal-like graphene papers, the thermally conductive materials with electrically insulating characteristic, namely decoupling of thermal and electrical transport properties, are increasingly significant in the electronics and energy systems such as solar power generation and light emitting diodes.[15,16] In targeted thermally conductive and electrically insulating applications, boron nitride (BN) and their derived materials have received broad interests for a variety of technological demands.[17-20] However, the remaining challenges including preparation of BN with controlled size, layer number and compatible interfaces still require considerable efforts for developing advanced BN-based composites of promoted thermal transport.[16,18] Very recently, for fabricating the thermally conductive materials of insufficient electrical conduction, manipulating the electrically conductive filler loading below the electrical percolation threshold coupled with acquiring substantially enhanced thermal transport properties appears to be an alternative strategy.[21] Based on this concept, Song et al. have recently fabricated the graphene/polymer composite films of two different transport properties, (i) sufficiently thermally conductive but electrically insulating in the sub-percolation graphene loadings (<20 vol%) and (ii) both highly thermally and electrically conductive beyond the percolation graphene loadings (>30 vol%).[21] Technically, the practical procedure appears similar to those for fabricating other graphene/polymer composites of enhanced thermal conductivity.[22-29] However, it is noted that the completely different changes observed in the electrical and thermal transport properties with increasing graphene fillers represent a remarkably meaningful plateau, allowing to design the advanced thermally conductive composites with variable electrical characteristics for various applications.[21]

In this contribution, we present a simply strategy to tune the interfaces of the electrically and thermally conductive multi-layer graphene nanosheets (GN) with electrically and thermally insulating graphene oxide (GO) nanosheets. With variable GN-to-GO ratio, the resulting flexible all-graphene papers possess highly tunable electrical and thermal transport properties in the entire semi-conductive range (10^{-7} S/m~10^{5} S/m). The unique electron and phonon transport behaviors at the anisotropic GN-GO interfaces has been discussed. Such all-graphene papers of extraordinary characteristics indicate an exceptional platform for tailing the thermally conductive materials in the semi-conductive graphene materials. The associated opportunities based on potential thermal management for wide applications have been discussed.

2. Experimental Section

2.1 Chemicals and materials.

The dialysis membranes of MWCO ≈ 3500 were supplied by Spectrum Laboratories and polyvinylidene fluoride (PVDF) filters with 0.45 μm pore size were provided from Fisher Scientific. The enhanced flake graphite powders were commercially purchased from Asbury Carbons. Concentrated H_2SO_4 (93%), H_2O_2 (35%), concentrated HNO_3 (73%), ethanol (EtOH), and P_2O_5 were supplied by Acros. $(NH_4)_2S_2O_8$ and $KMnO_4$ powders were from Aldrich.

2.2 Fabrication of GN papers.

GN papers were fabricated according to our previous work.[13] Briefly, the raw graphite powders (1 g) was processed in a aqueous EtOH mixture solution (260 mL EtOH and 140 mL H_2O) for stirring and sonication overnight. Upon treatment, the samples were dried in a vacuum oven. The as-treated samples (0.5 g) were further exfoliated in the mixed acid solution of H_2SO_4 and HNO_3 with 3:1 v/v (80 mL) under the sonication for 2 days. The

processed mixed suspension was then transferred into 2 L water for dilution, and was subsequently washed with water and EtOH until the pH reached 7. A portion of the clean suspension was then transferred onto the PVDF filter under the vacuum, allowing the GN powders to be aligned for forming the GN papers.

2.3 Fabrication of GO papers.

GO papers were fabricated from the directly filtrated the GO solution. The GO was prepared according the minor modified Hummer's method. [13,30] Briefly, H_2SO_4 (93%, 10 mL) was heated to 80 °C, followed by adding $(NH_4)_2S_2O_8$ (0.9 g) and P_2O_5 (0.9 g). Until the reagents were completely dissolved, the graphite powders (1 g) were added, and the mixed suspension was heated at 80 °C for 4.5 h. After cooling to room temperature, the mixture was diluted with water (250 mL) and kept overnight. The processed mixture was washed with H_2O and dried in the oven. The dried powders was then added into H_2SO_4 (93%, 40 mL) in a flask cooled in an ice bath. $KMnO_4$ powders (5 g over 40 min) was carefully added into the mixed suspension and the temperature was kept at lower than 10 °C. The mixture was heated up 35 °C for 2 h, followed by dilution with water and further stirring for 2 h. The mixture was then transfer into in 250 mL and was added with aqueous H_2O_2 (30%, 10 mL), followed by settling overnight. The sediment was washed with mixture aqueous solution of H_2SO_4 (5 wt%)-H_2O_2 (0.5 wt%) and HCl solution (10 wt%). Upon repeated washing with water until no layer separation after centrifugation, the processed sample was then dialyzed (MWCO ~ 3,500) in the water for a week to yield a clean aqueous GO solution. A portion of the as-prepared GO solution was directly transferred onto the PVDF filter to achieve GO papers upon vacuum condition.

2.4 Fabrication of GN/GO papers.

In the preparation of GN/GO papers, a portion of GN papers was added into the GO solution, where GN loadings changes in the range from 20 to 80 wt% in the composite papers.

The mixture was then sonicated with a tip-sonication, allowing the GN paper to re-disperse in the GO solution. Until stable suspension was obtained, the mixture was subsequently processed onto the PVDF filter to fabricate GN/GO papers under the vacuum condition. Upon drying in the oven, the resulting samples were peeled off from the PVDF filter to achieve GN/GO papers.

2.5 Characterizations.

Scanning electron microscopy (SEM) images were obtained on the Hitachi S-4800 field-emission SEM system. Transmission electron microscopy (TEM) images were carried out on Hitachi HD-2000 Scanning-TEM system and Hitachi H-9500 TEM system. In the TEM specimen preparation, a paper sample was embedded in epoxy resin, followed by microtoming with a 30° angle diamond knife (Reichert-Jung Ultracut E Microtome) for achieving slices of cross-sectional with respect to the original film surface (less than 100 nm in thickness). Raman spectra were performed on a Raman spectrometer (Jobin Yvon T64000) equipped with a 35 mW He-Ne laser source (Melles-Griot) for 633 nm excitation. X-ray diffraction (XRD) measurements were carried out on a Scintag XDS-2000 powder diffraction system. X-ray photoelectron spectroscopy (XPS) was performed on a Thermo Fisher Scientific ESCALAB system.

The electrical conductivity of the papers was measured by using the classical four-probe method on the setup consisting of a multimeter (Keithley 2400 controlled by Lab Tracer 2.0 software, both from Keithley Instruments) and a multi-height probe (Jandel). The electrical conductivity (σ) value was calculated according to the equation $\sigma = (\ln 2/\pi)(I/V)/d$, where d, I and V denotes the paper thickness, electrical current and voltage, respectively. Each paper was measured based on multiple spots and the average values and errors were taken for each sample.

The in-plane thermal conductivity (κ) of the papers was achieved based on the in-plane thermal diffusivity (α), specific heat (C_p) and density (ρ), according to the relation $\kappa = \alpha C_p \rho$. The specific heat of GN and GO was generally available from that of graphitic materials (0.71 J/g·K). The density of the papers was approximately obtained according to ratio of the mass to the dimensions, with a range of 1.5 ~ 1.7 g/cm^3 in the measurement. The in-plane thermal diffusivity of the papers was acquired on an Ulvac LaserPIT thermal diffusivity/conductivity meter. The measurement was operated at room temperature in a vacuum of 0.01 Pa and with the use of multiple frequencies. The copper standard (0.25 mm in thickness) was supplied with the instrument, which was used as the reference sample. All of the as-fabricated papers were cut into rectangular pieces of 30 mm × 5 mm in dimension with thickness less than 0.03 mm. Commercial silver paste was used as the binder to connect the testing papers being tested with the sensor in the testing holder of the instrument.

3. Results and Discussion

The all-graphene papers were fabricated based on various approaches for exfoliating graphite coupled with subsequent alignment of the resulting graphene nanosheets. In the typical process of the GN paper (Figure 1),[13] the graphite was directly expanded and exfoliated via the liquid phase method. Upon the long-term sonication in the mixed acid solution, graphite was exfoliated into electrically and thermally conductive GN nanosheets, followed by being aligned into the anisotropic GN paper via the vacuum-supported filtration. For the GO paper, the graphite was treated by the minor modified Hummers' methods,[13,30] allowing it to be oxidized and exfoliated into electrically and thermally insulating GO nanosheets (Figure 1). The subsequent filtration was carried out to align the GO nanosheets to form the GO paper. In the typical preparation of GN/GO papers with tunable thermal and electrical transport properties, GN and GO nanosheets in various mass ratios were

homogeneously dispersed in the aqueous solution, followed by alignment with the filtration (Figure 1).

The as-fabricated anisotropic all-graphene papers were cut into slices for characterizations with various techniques. As shown in Figure 2A-2C, the all-graphene papers are mechanically flexible as expected. The GN paper presents metal-like appearance and the GO paper appears brownish. Typical SEM images of these all-graphene papers are given in Figure 2D-2F, showing that the GN/GO paper (50 wt% GN, Figure 2E) appear similar anisotropic characteristic to both GN (Figure 2D) and GO papers (Figure 2F). Since the hydrophilic functional groups in both GN and GO nanosheets are favorable to interact with water for forming hydrogen bonding, these nanosheets could be well uniformly dispersed in the aqueous solution. As a result, GN and GO nanosheets are able to be homogeneously stacked into GN/GO papers as schemed in Figure 2H, analogous to the anisotropic stacking in both GN and GO papers. The cross-sectional TEM views of the microtomed samples are exhibited in Figure 3. Representative TEM images demonstrate that the GN nanosheets of several nanometers in thickness have been well aligned in the GN paper (Figure 3A), with similar observation in the GO paper stacked with few-layer GO nanosheets (Figure 3B). As shown in Figure 3C and 3D, combination of GN and GO nanosheets also well maintains the similar stacking feature, which is consistent with the SEM results.

Figure 4A exhibits the XRD spectra of the all-graphene papers. As expected, a shifted peak (~10^{o}) with no graphitic peak was observed in the GO paper, in agreement with the other GO by the Hummers' method.[31] The GN paper shows a graphitic peak (002) around 26^{o}, and the GN/GO paper (50 wt% GN loading) presents superposition of the diffraction peaks originated from both GN and GO papers. According to Raman spectra shown in Figure 4B, all the graphene-based papers exhibit D-band and G-band at 1340 cm^{-1} and 1585 cm^{-1},

respectively. Additionally, GN paper appears sharper G-band caused by the enhanced Raman signal relative to GO paper since the latter is relatively colorless and the former has absorption at the Raman excitation wavelength based on the extended GN network. It is observed that the broadened D-band and G-band have been delivered into the GN/GO papers.

The chemical compositions of the samples were obtained on the XPS. According to the XPS spectra (Figure 4C), elemental concentrations of C, O and N in the GN paper were measured to be 90.36%, 8.71% and 0.93%, respectively, in comparison with 62.65%, 36.53% and 0.82% in the GO paper. As expectation, the GN/GO paper (50 wt% GN loading) has 77.35%, 21.79% and 0.86% for the C, O and N elements, respectively. On the basis of fitting the C1s spectra in Figure 4D, the peaks located around 285, 286, 288 and 289 eV are assigned to be carbon-carbon, –C–O, –C=O and –O–C=O species, respectively.[32] As is aforementioned, these hydrophilic functional groups are responsible for creating the hydrogen bonding networks between the nanosheets and water, allowing the floating nanosheets to be aligned under the compression from the air–water interface upon filtration. In addition, the GO paper appears much broader carbon-carbon peaks than the GN paper, due to the conversion of sp2 hybridized carbon into sp3 hybridized carbon (red shift in the spectra) in the oxidation process.[32,33] Moreover, the GO paper of much higher O concentration possesses a large amount of oxygen-containing functional groups (e.g. carboxyl, carbonyl and hydroxyl groups) owing to the harsh oxidization. In contrast, the GN paper that possesses higher intensity in the sp2 hybridized carbon peak presents much smaller concentration in the oxygen-containing functional groups. Due to the tremendously different chemical compositions between GN and GO, the chemical compositions and GN-GO interfaces of the resulting GN/GO papers could be varied via changing the GN-to-GO ratios (Figure 4D).

The electrical conductivity of the all-graphene papers have been measured based on the classical four-probe method. As shown in Figure 5A, the electrical conductivity of the all-graphene papers ranges from the order of ~10^{-7} S/m to that of 10^{4} S/m, depending on the GN loading in the paper. Note that the electrical conductivity of the GO paper is almost insulating because the conjugated structures based on sp2 hybridized carbon have been largely damaged in the harsh oxidation. Thus, GO nanosheets play a similar role to insulating polymer matrices and GN nanosheets, on the contrary, are the conductive fillers. As shown in Figure 5C, the enhancements in electrical conductivity are given based on the calculation of the value achieved in the GO paper, suggesting an extreme enlargement up to ~10^{12} fold.

Interestingly, the inset of Figure 5A suggests that the logarithm values of electrical conductivity present approximately linear enhancement with increasing GN loading. Such unique linear increment is rarely observed in other carbon/polymer composites since the increment of the electrical conductivity in the polymeric composites generally obeys the percolation theory as follow: [34-36]

$$\sigma \propto (x - x_c)^{\beta}, \quad (1)$$

where σ is the electrical conductivity of composites, x the filler content ($x>x_c$), x_c the percolation threshold where the transition takes place, and β the critical exponent for the conductivity. In practice, the β that depends on the system dimensionality is known to be 1.3 and 1.94 for ideal two-dimensional and three-dimensional systems, respectively.[21,35,36] According to the GN/polymer composites in our previous work, critical exponent was found to be ~1.26 and the percolation threshold was around ~20 vol% (also 36 wt%).[21] However, no pronounced two-dimensional percolation threshold characteristic was observed in the GN/GO system.

In semiconductors, electrical conductivity (σ) could be briefly described as below[37]

$$\sigma = n\, e\, \mu, \quad (2)$$

where n is the carrier concentration and μ the carrier mobility that is known to be given as[37]

$$\mu \approx e\,\tau_E / m^*, \quad (3)$$

where τ_E is electron scattering relaxation time and m^* the electron effective mass. In the GN/GO papers, n is mainly determined by the GN loading; on the other hand, μ along with τ_E is primarily dependent on the electron scattering on the graphene planes and electron scattering at the exceptionally anisotropic all-graphene interfaces, which leads to the exclusive electrical properties. Schemes demonstrated in Figure 6A-6C are the electrical transport behaviors of the all-graphene interfaces. According to the characterizations, the GN nanosheets, whose sp2 hybridized carbon and corresponding in-plane electronic transport paths have been largely preserved, are highly electrically conductive. As a consequence, free electrons are able to fast travel on both GN planes and GN-GN interfaces due to the limited electron scattering (heteroatom concentration<10%, XPS results) (Figure 6A). Moreover, the electrically insulating GO maintains a fraction of isolated conductive regions, which are linked to the residual sp2 hybridized carbon. These special isolated conductive regions could not substantially change the electrically insulating feature of GO-GO interfaces in the GO papers (Figure 6C). In the GN-GO interfaces, however, they are able to serve as the conductive bridges that allow the hopping electrons to travel through the GN-GO interfaces (Figure 6B). In this case, the insulating GO nanosheets play an exceptional role on the electron transport in the GN-GO papers, which thus present an extraordinarily unique electrical characteristic compared to the conventional polymer composites with carbon fillers.

The thermal conductivity of the all-graphene papers were achieved according to the calculation of in-plane thermal diffusivity, specific heat and density, where the errors originate from the measurement of thermal diffusivity and density. Shown in Figure 5B is the thermal conductivity of the all-graphene papers with the increasing GN loading. As is anticipated, the thermal conductivity was almost linearly enhanced with the increase of GN

loading in the all-graphene papers, ranging from average values ~0.6 W/mK in the GO papers to ~135 W/mK in the GN papers. The corresponding enhancements in the GN/GO papers were calculated based on the value of GO paper (Figure 5D), indicating the thermally conductive papers present up to 22000-fold higher thermal conductivity than the GO paper.

The monotonic change in the thermal conductivity is also attributed to the introduction of GO interfaces in the anisotropic graphene papers. In theory, thermal conductivity (κ) is a property of material to transport heat, which follows Fourier's law[5]

$$Q = -\kappa \nabla T, \quad (4)$$

where Q is the heat flux and ∇T the temperature gradient through the medium, and the negative sign suggests the heat flux from high to low temperature.[5] The thermal conductivity refers to the specific heat (C_p), averaged phonon group velocity (v) and phonon mean free path (λ), following the relation as[5]

$$\kappa \approx \Sigma C_p v \lambda. \quad (5)$$

In the all-graphene papers, it is suggested that the thermal conductivity could be dominantly determined by the phonon mean free path. The presence of boundaries, defects and other phonons induced by the heteroatoms can generate the phonon scatterings, which results in shortening the phonon mean free path.[5,38] Phonon scattering mechanisms can be characterized by the inverse of the relaxation time $1/\tau$, and the corresponding combined relaxation time τ_c in the all-graphene papers can be described as

$$1/\tau_c \approx 1/\tau_m + 1/\tau_b + 1/\tau_{p\text{-}p}, \quad (6)$$

where τ_m, τ_b and $\tau_{p\text{-}p}$ represents mass-difference impurity scattering, boundary scattering and phonon-phonon scattering within an individual graphene layer, respectively. As demonstrated in Figure 6D-6F, the mass-difference impurity scattering mainly induced by the increased oxygen concentration and defect is responsible for the enlarged mass-difference impurity scattering in the GN/GO papers, compared to the GN papers of much smaller oxygen

concentration. [5, 39-41] Furthermore, boundary scattering is specifically significant in the two-dimensional nanoscale materials. Theoretically, a specular scattering could be achieved in a smooth perfect surface, and whereby boundary scattering has no impact on the thermal transport. Due to the larger amount of heteroatoms and defects, the GO nanosheets of rougher edges contribute greater boundary scattering than GN nanosheets. Meanwhile, the presence of graphene-based interfaces, consisting of GN-GN, GN-GO and GO-GO interfaces with different interface scattering features, lead to various phonon-interface scatterings.[39-41] In addition, the overlap of graphene layers, GN-GN, GN-GO and GO-GO stacking, would generate out-of-plane phonon–phonon scattering.[5,38] Owing to the larger thickness in GN, namely more graphitic feature, the GN paper based on GN-GN stacking is suggested to present reduced out-of-plane phonon–phonon scattering. In the nutshell, the results indicate that the utilization of GO nanosheet as a unique interface plays a critical role in tuning the electrical and thermal transport in the all-graphene papers.

As exhibited in Figure 7A, a plot of electrical conductivity-to-thermal conductivity ratio against the GN loading in the all-graphene papers is given. The enhancements in thermal and electrical transport were essentially monotonic (inset of Figure 7A), which indicates that the employment of a GO interface in the GN stacking system appears much greater impact on the electrical conductivity. As a consequence, an exceptional stage for electrically insulating materials with sufficiently enhanced thermal transport properties could be achieved in the region of smaller GN loading, which is schematically demonstrated in Figure 7B.

More importantly, the GN/GO papers hold highly unique properties with taking accounting of both electrical and thermal conductivity, as shown in Figure 7C. In the region of insulators, the polymeric composites embedded with boron nitride are widely used in the heat dissipation and thermal management, where electrical insulation is a fairly critical

requirement.[15-19] Beyond this region, the conventional metals of superior electrical and thermal conduction are also applied, but limited to the fields where lightweight, anti-corrosion, anti-oxidation and chemical stability are needed. Thus, graphene/polymer composites are very promising because of their special advantages. According to the comparison based on the recent polymeric ones (Figure 7C),[21-29,42] the GN/GO papers in this work present a highly broad tunable range in both electrical and thermal conductivity, with considerably enhanced thermal transport properties achieved. These extraordinary properties are mainly attributed to several particular characteristics. (i) The directly exfoliated GN of few-layer feature enables the inner graphitic layers to maintain highly electrical and thermal transport properties, and thus sufficient thermal conductivity could be realized at small GN loading. (ii) The process for fabricating the all-graphene papers is practically simple and controllable. Upon the GN loadings from 0 to 100 wt%, the electrical conductivity of the all-graphene papers could be manipulated in the entire range of semiconductors (10^{-7}~10^{5} S/m) (Figure 7C). In the contrary, it is generally difficult to achieve polymeric composites of extremely high filler loadings because of the limitation in the polymer processing. (iii) In the polymeric composites with homogeneous fillers, a specific alignment is usually required to obtain the anisotropic characteristic, aiming to approaching the optimal thermal transport properties.[17] In contrast, the all-graphene papers that are intrinsically anisotropic possess the ideal feature for facilitating the phonon transport. Based on the recent literature (Table S1), direct comparison of the values in thermal conductivity further suggests that such all-graphene papers are more prone to be controlled for achieving highly thermally conductive feature.

As the ultimate performance of the all-graphene papers (Figure 7C), thermally treated graphene papers in recent report present superior electrical and thermal conductivity owing to substantial removal of oxygen-containing functional groups coupled with well recovery of

sp2 hybridized carbon under the extreme conditions.[10-14] They are expected to serve as the potential substitutes for conventional metals and alloys. On the other hand, the thermally conductive all-graphene papers with tunable electrical properties in the entire semi-conductive range are particularly important in the thermal management of electronics and semiconductor industry.

Conclusions

In summary, two different graphene nanosheets, electrically and thermally conductive GN as well as electrically and thermally insulating GO, were utilized to fabricate all-graphene papers. In the entire semi-conductive range, tunable electrical and thermal properties could be simply achieved via controlling the ratio of GN to GO. The unique all-graphene papers with monotonically increased electrical characteristic and linear enhanced thermal conductivity were found to be determined by the introduction of GO interfaces in the resulting anisotropic graphene stacking. The fundamental mechanisms coupled with unique electron and phonon transport properties suggest that the all-graphene papers promise great potential in the thermal management for wide applications.

Acknowledgment

This research was supported by the National Natural Science Foundation of China (51377096 and 51102007), the China Postdoctoral Science Foundation (2014M560934) and the Fundamental Research Funds for the Central Universities (2015QN16).

References

[1] A. A. Balandin, *Nat. Mater.*, 2011, **10**, 569–581.

[2] S. S. Chen, Q. Z. Wu, C. Mishra, J. Y. Kang, H. J. Zhang, K. J. Cho, W. W. Cai, A. A. Balandin and R. S. Ruoff, *Nat. Mater.*, 2012, **11**, 203–207.

[3] S. Ghosh, W. Z. Bao, D. L. Nika, S. Subrina, E. P. Pokatilov, C. N. Lau and A. A. Balandin, *Nat. Mater.*, 2010, **9**, 555–558.

[4] W. L. Song, L. M. Veca, A. Anderson, M. S. Cao, L. Cao and Y.-P. Sun, *Nanotechnol. Rev.,* 2012, **1**, 363–376.

[5] E. Pop, V. Varshney and A. K. Roy, *MRS Bull*, 2012, **37**, 1273–1281.

[6] A. A. Balandin, S. Ghosh, W. Z. Bao, I. Calizo, D. Teweldebrhan, F. Miao and C. N. Lau, *Nano Lett.,* 2008, **8**, 902–907.

[7] L. M. Veca, M. J. Meziani, W. Wang, X. Wang, F. S. Lu, P. Y. Zhang, Y. Lin, R. Fee, J. W. Connell and Y.-P. Sun, *Adv. Mater.*, 2009, **21**, 2088–2092.

[8] L. L. Tian, P. Anilkumar, L. Cao, C. Y. Kong, M. J. Meziani, H. J. Qian, L. M. Veca, T. J. Thorne, K. N. Tackett, T. Edwards and Y.-P. Sun, *ACS Nano*, 2011, **5**, 3052–3058.

[9] Q. Li, Y. F. Guo, W. W. Li, S. Q. Qiu, C. Zhu, X. F. Wei, M. L. Chen, C. J. Liu, S. T. Liao, Y. P. Gong, A. K. Mishra and L.W. Liu, *Chem. Mater.*, 2014, **26**, 4459−4465.

[10] J. L. Xiang and L. T. Drzal, *Carbon*, 2011, **49**, 773–778.

[11] G. M. Yuan, X. K. Li, Z. J. Dong, A. Westwood, Z. W. Cui, Y. Cong, H. D. Du and F. Y. Kang, *Carbon*, 2012, **50**, 175–182.

[12] Q. Z. Liang, X. X. Yao, W. Wang, Y. Liu and C. P. Wong, *ACS Nano*, 2011, **5**, 2392–2401.

[13] Z. L. Hou, W. L. Song, P. Wang, M. J. Meziani, C. Y. Kong, A. Anderson, H. Maimaiti, G. E. LeCroy, H. J. Qian and Y.-P. Sun, *ACS Appl. Mater. Interfaces*, 2014, **6**, 15026−15032.

[14] B. Shen, W. T. Zhai and W. G. Zheng, *Adv. Funct. Mater.*, 2014, **24**, 4542–4548.

[15] X. Y. Huang, C. Y. Zhi, P. K. Jiang, D. Golberg, Y. Bando and T. Tanaka, *Adv. Funct. Mater.*, 2013, **23**, 1824–1831.

[16] M. J. Meziani, W. L. Song, P. Wang, F. S. Lu, Z. L. Hou, A. Anderson, H. Maimaiti and Y.-P. Sun, *Chemphyschem*., 2015, **16**,1339–1346.

[17] W. L. Song, P. Wang, L. Cao, A. Anderson, M. J. Meziani, A. J. Farr and Y.-P. Sun, *Angew. Chem. Int. Ed.*, 2012, **51**, 6498–6501.

[18] A. Pakdel, Y. Bando and D. Golberg, *Chem. Soc. Rev.*, 2014, **43**, 934–959.

[19] Z. Y. Lin, A. Mcnamara,Y. Liu, K. S. Moon and C. P. Wong, *Compos. Sci. Technol.*, 2014, **90**, 123–128.

[20] H. L. Zhu, Y. Y. Li, Z. Q. Fang, J. J. Xu, F. Y. Cao, J. Y. Wan, C. Preston, B. Yang and L. B. Hu, *ACS Nano*, 2014, **8**, 3606–3613.

[21] W. L. Song, L. M. Veca, C. Y. Kong, S. Ghose, J. W. Connell, P. Wang, L. Cao, Y. Lin, M. J. Meziani, H. J. Qian, G. E. LeCroy and Y.-P. Sun, *Polymer*, 2012, **53**, 3910–3916.

[22] S. H. Song, K. H. Park, B. H. Kim, Y. W. Choi, G. H. Jun, D. J. Lee, B. S. Kong, K. W. Paik and S. Jeon, *Adv. Mater.*, 2013, **25**, 732–737.

[23] M. C. Hsiao, C. C. M. Ma, J. C. Chiang, K. K. Ho, T. Y. Chou, X. F. Xie, C. H. Tsai, L. H. Chang and C. K. Hsieh, *Nanoscale*, 2013, **5**, 5863–5871.

[24] M. Safdari and M. S. Al-Haik, *Carbon*, 2013, **64**, 111–121.

[25] X.Y. Huang, C.Y. Zhi and P. K. Jiang, *J. Phys. Chem. C*, 2012, **116**, 23812−23820.

[26] R. Wang, D. X. Zhuo, Z. X. Weng, L. X. Wu, X. Y. Cheng, Y. Zhou, J. L. Wang and B.W. Xuan, *J. Mater. Chem. A*, 2015, **3**, 9826–9836.

[27] C. C. Teng, C. C. M. Ma, C. H. Lu, S. Y. Yang, S. H. Lee, M. C. Hsiao, M. Y. Yen, K. C. Chiou and T. M. Lee, *Carbon*, 2011, **49**, 5107–5116.

[28] F.Yavari, H. R. Fard, K. Pashayi, M. A. Rafiee, A. Zamiri, Z. Z. Yu, R. Ozisik, T. Borca-Tasciuc and N. Koratkar, *J. Phys. Chem. C*, 2011, **115**, 8753–8758.

[29] S. H. Lee, J. H. Jung and IK. Oh, *Small*, 2014, **10**, 3880–3886.

[30] W. S. Hummers and R. E. Offeman, *J. Am. Chem. Soc.*,1958, **80**, 1339–1339.

[31] L. L. Tian, M. J. Meziani, F. S. Lu, C. Y. Kong, L. Cao, T. J. Thorne and Y.-P. Sun, *ACS Appl. Mater. Interfaces*, 2010, **2**, 3217–3222.

[32] S. Stankovich, D. A. Dikin, R. D. Piner, K. A. Kohlhaas, A. Kleinhammes, Y. Jia, Y. Wu, S. T. Nguyen, R. S. Ruoff, *Carbon* 2007, 45, 1558–1565.

[33] A. Hunt, D. A. Dikin, E. Z. Kurmaev, T. D. Boyko, P. Bazylewski, G. S. Chang and A. Moewes, *Adv. Funct. Mater.*, 2012, **22**, 3950–3957.

[34] N. Li, Y. Huang, F. Du, X. B. He, X. Lin, H. J. Gao, Y. F. Ma, F. F. Li, Y. S. Chen and P. C. Eklund, *Nano Lett.*, 2006, **6**, 1141–11145.

[35] W. Bauhofer and J. Z. Kovacs, *Compos. Sci. Technol.*, 2009, **69**, 1486–1498.

[36] W. Wang, K. A. S. Fernando, Y. Lin, M. J. Meziani, L. M. Veca, L. Cao, P. Zhang, M. M. Kimani and Y.-P. Sun, *J. Am. Chem. Soc.*, 2008, **130**, 1415–1419.

[37] J. H. Yang, H. L. Yip and A. K. Y. Jen, *Adv. Energy Mater.*, 2013, **3**, 549–565.

[38] M. S. Ahmed, S. Ezugwu, R. Divigalpitiya and G. Fanchini, *Carbon*, 2013, **61**, 595–601.

[39] Y. S. Xie, Z. L. Xu, S. Xu, Z. Cheng, N. Hashemi, C. Deng and X. W. Wang, *Nanoscale*, 2015, **7**, 10101–10110.

[40] S. X. Zhou, J. Z. Xu, Q. H.Yang, S.W.Chiang, B. H. Li, H. D. Du, C. J. Xu and F. Y. Kang, *Carbon*, 2013, **57**, 452–459.

[41] X. Shen, X. Y. Lin, J. J. Jia, Z. Y. Wang, Z. G. Li and J. K. Kim, *Carbon*, 2014, **80**, 235–245.

[42] W. L. Song, W. Wang, L. M. Veca, C. Y. Kong, M. S. Cao, P. Wang, M. J. Meziani, H. J. Qian, G. E. LeCroy, L. Cao, Y.-P. Sun, *J. Mater. Chem.* 2012, **22**, 17133–17139.

Figure captions

Figure 1. Scheme for fabricating the all-graphene papers of various electrical and thermal properties.

Figure 2. Optical photos of the GN (A), GN/GO (B) and GO papers (C); cross-section SEM views of the GN (D), GN/GO (50 wt% GN loading) (E) and GO papers (F); Schemes of the cross-section views of the GN (G), GN/GO (H) and GO papers (I).

Figure 3. Microtomed TEM images for the cross-section views of GN (A), GO (B) and GN/GO papers (50 wt% GN loading) (C and D).

Figure 4. XRD (A), Raman (B) and XPS spectra (C) of the samples as marked; XPS C1s spectra of the samples as marked, where GN/GO papers are 1:1 in weight ratio (D).

Figure 5. Electrical conductivity (A) and thermal conductivity (B) of the all-graphene papers; enhancements in electrical conductivity (C) and thermal conductivity (D) based on the corresponding values in the GO paper.

Figure 6. Schemes of electron and phonon transport at GN-GN (A and D), GN-GO (B and E) and GO-GO (C and F) interfaces.

Figure 7. Electrical conductivity-to-thermal conductivity ratio against the GN loading (A); thermally conductive all-graphene papers with different electrical transport properties (B); recent advances in the thermally conductive materials of different electrical properties (C).

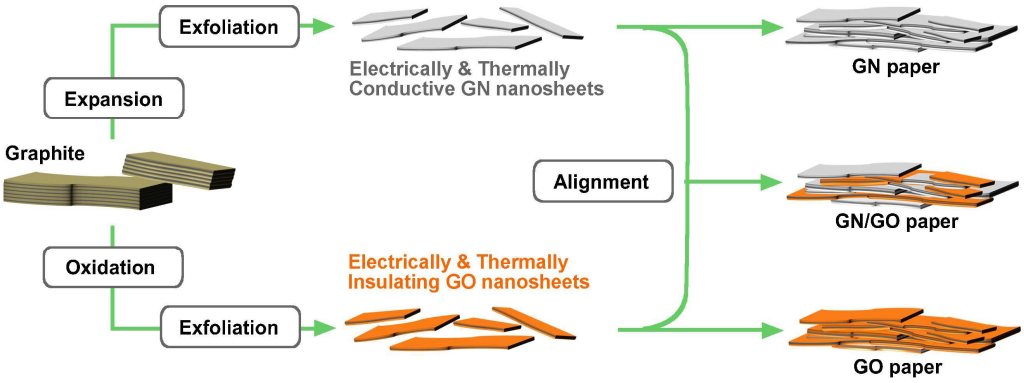

Figure 1.

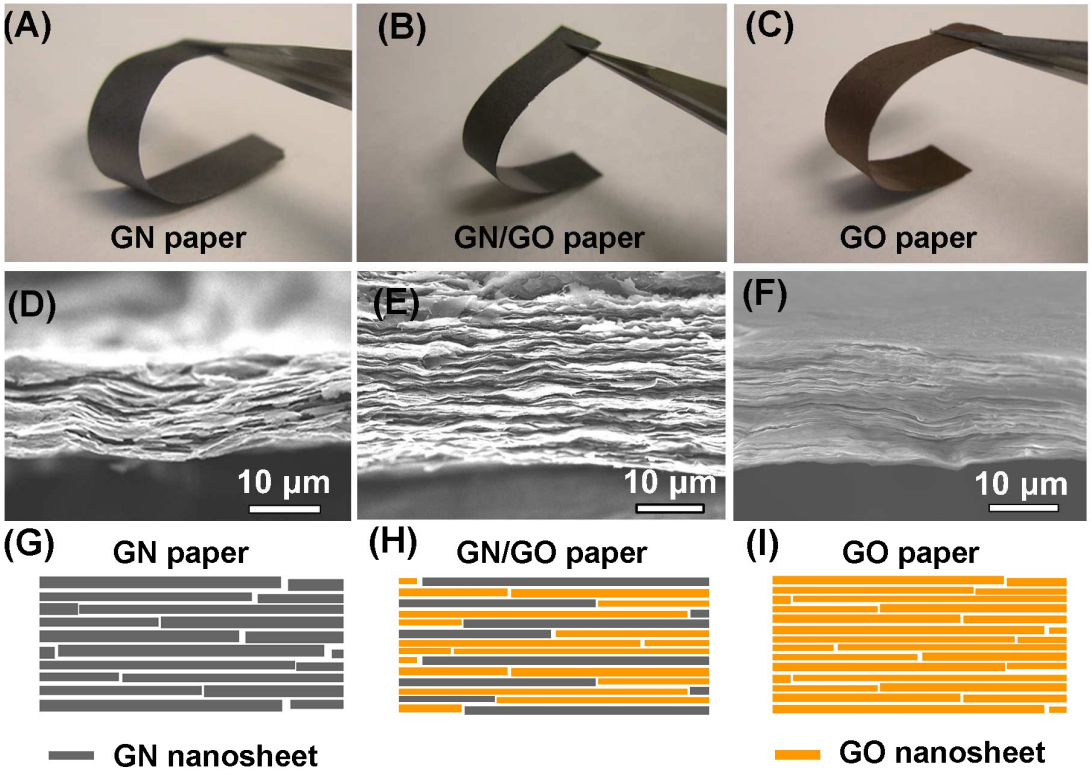

Figure 2.

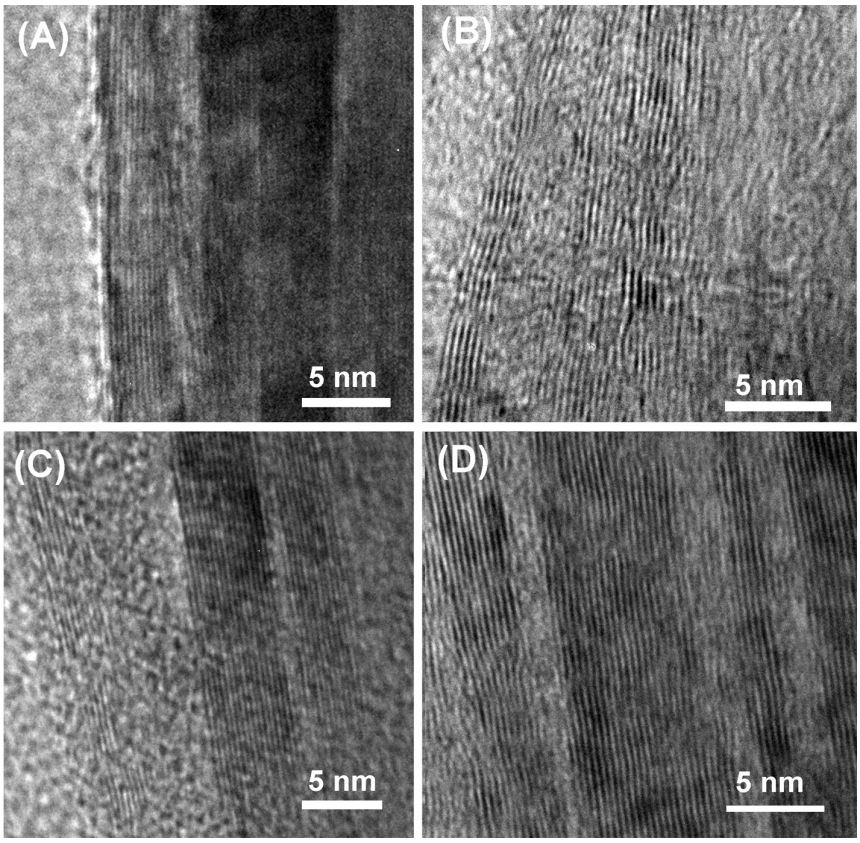

Figure 3.

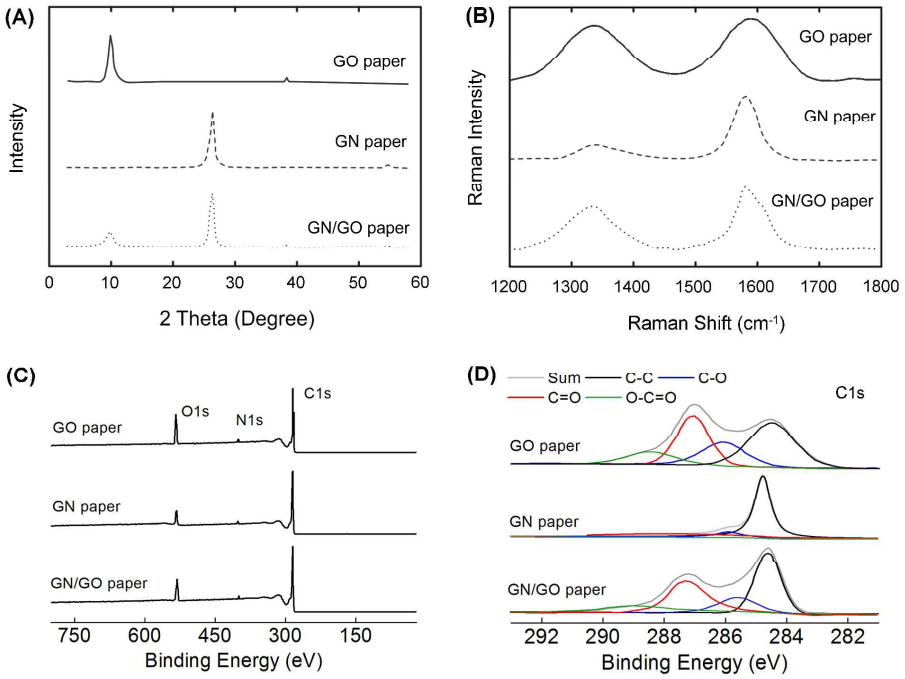

Figure 4.

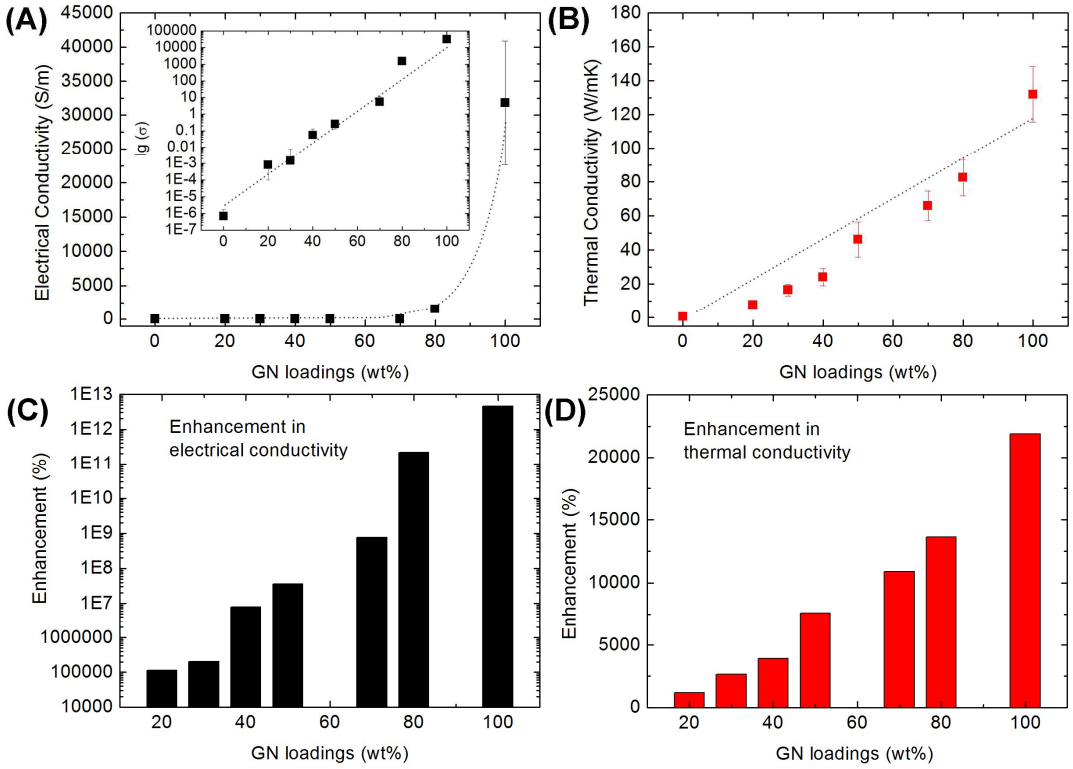

Figure 5.

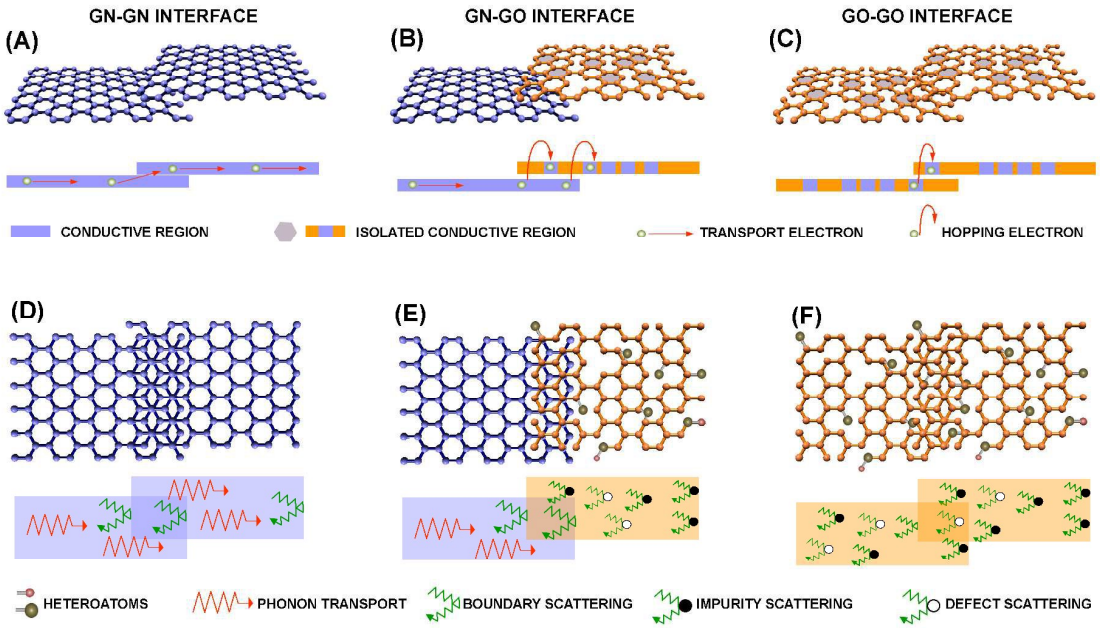

Figure 6.

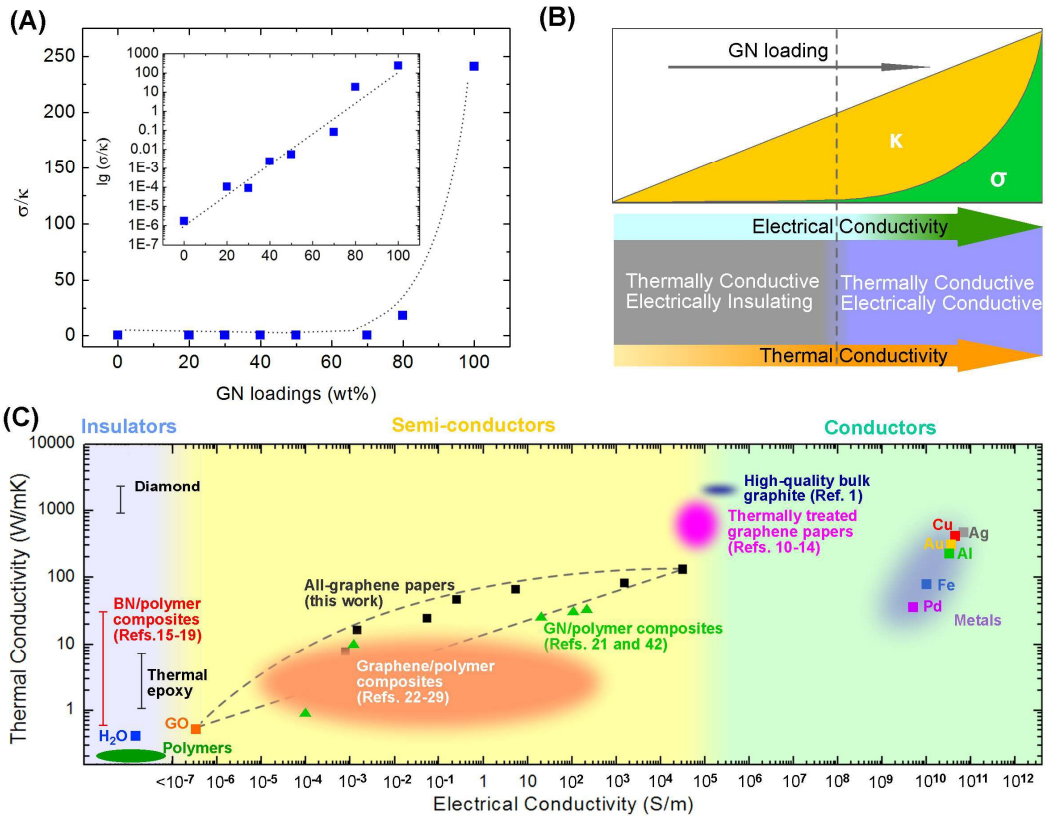

Figure 7.